rupole-split doublet was observed in the rubidium system. This is shown in Figure 4b. The corresponding X-ray powder diffraction data indicated the presence of CsAu and CsCN in the cesium system, and RbCN and a pattern different from that of any of the known phases in the Rb–Au system (RbAu, $RbAu_2$, and $RbAu_4$). The identity of this phase will be discussed below.

As noted above, solutions of RbAu and CsAu in liquid NH_3 are unstable over prolonged periods of time, even in the presence of excess alkali metal. Hydrogen is generated, and in both cases solids form. Solutions of CsAu and RbAu were therefore allowed to decompose at room temperature, and another containing RbAu was allowed to decompose at −30 to −40 °C. The ^{197}Au Mössbauer spectra of the products in the rubidium system were somewhat complicated. For the solution allowed to decompose at room temperature, the spectrum consisted of a single line with an isomer shift identical with that of gold metal and a quadrupole-split doublet, with contributions of 37.3 and 62.7%, respectively. The isomer shift and quadrupole splitting for the doublet were identical with those for the phase obtained on stripping the solvent from a solution of RbAu, in the presence of rubidium, at −50 °C. The solution allowed to decompose at −30 °C gave a solid product for which the ^{197}Au Mössbauer spectrum was dominated by the same quadrupole doublet as above but was further complicated by at least two components at lower isomer shift, which may account for up to 30% of the spectral intensity. Lack of resolution, and of a suitable model, prevent unambiguous assignment of parameters for these components. In either case, X-ray powder photographs showed only the presence of the pattern attributable to the phase obtained on stripping the solvent from an RbAu solution at low temperatures. This would suggest that little elemental gold is actually present in the samples obtained after decomposition at room temperature or low temperature, unless it is in an amorphous form. Also, because of the higher recoil-free fraction of elemental gold compared to the alkali-metal–gold phases studied in this work the relative contribution of the gold metal resonance to the ^{197}Au Mössbauer spectra of these samples would exceed the actual relative abundance of gold metal. Chemical analysis of the solid obtained on decomposition at room temperature indicated a composition of $RbAu_{1.7(1)}$, in apparent agreement with the composition of the K–Au phase obtained in a related reaction described above. Even if 30% of the gold in this sample were present as elemental gold, the remaining intermetallic would still possess a composition intermediate between RbAu and $RbAu_2$. It would appear, therefore, that just as was found for the K–Au system, a new and perhaps similar phase exists in the Rb–Au system that lies between RbAu and $RbAu_2$. The ^{197}Au Mössbauer spectra for the two systems (Figure 4) yield parameters (Table II) that are closely comparable; the potassium intermetallic gives the lower isomer shift, consistent with the relative electronegativities of the alkali metal. Moreover, their X-ray powder diffraction patterns, although not indicating isomorphicity, were strikingly similar. These phases appear to be inaccessible by a high-temperature synthetic method.

In the cesium system the sole product from decomposition of the NH_3 solution of CsAu at room temperature, detectable by X-ray powder photography, was gold metal. The ^{197}Au Mössbauer spectrum showed an intense single line whose isomer shift is identical with that for pure gold but also contained a very weak signal, <10% of the total spectral intensity, centered at approximately 6.4 mm s^{-1} relative to elemental composition between that of Au and CsAu. No such phases are reported in the binary phase diagram for the Cs–Au system.[18,22] Earlier workers[17] have also detected a resonance between those for Au and CsAu (at approximately 2.3 mm s^{-1} relative to gold) when recording the spectrum of an impure sample of CsAu. It is possible that these weak signals represent the two components of a quadrupole doublet analogous to those found by us for the intermediate phases in the K–Au and Rb–Au systems. Since this intermediate CsAu phase is a minor component in either the spectrum of CsAu[17] or in that resulting from oxidation by NH_3 of CsAu, one of the components of the postulated quadrupole doublet would be concealed by the flanks of either the Au or the CsAu resonances. We find that a component with parameters δ = 4.0 (1) mm s^{-1} and Δ = 4.6 (2) mm s^{-1} gives the best agreement with our experimental data. However, it appears that any phases intermediate between Au and CsAu are much less stable and more susceptible to oxidation to gold metal than are analogous phases in the rubidium and potassium systems.

Acknowledgment. We thank the Natural Sciences and Engineering Research Council of Canada for financial support, Dr. G. J. Schrobilgen for the use of the inert atmosphere box facilities, J. D. Garrett, for fabrication of the molybdenum crucibles, Dr. J. W. Harvey, senior Health Physicist, and M. P. Butler and the staff of the McMaster Nuclear Reactor for help with neutron irradiations.

Contribution from the Kenan Laboratories of Chemistry, The University of North Carolina, Chapel Hill, North Carolina 27514

Synthesis and Redox Properties of a Bipyridyl Analogue of Ruthenium Red

Daniel A. Geselowitz, Wlodzimierz Kutner,† and Thomas J. Meyer*

Received August 19, 1985

The preparation of the new compound bis[(μ-oxo)-*cis*-aquabis(bipyridine)ruthenium]-*trans*-bis(bipyridine)ruthenium(6+) perchlorate, with the formula $[(bpy)_2(H_2O)Ru^{III}ORu^{IV}(bpy)_2ORu^{III}(OH_2)(bpy)_2](ClO_4)_6$ (bpy = 2,2′-bipyridyl), is reported. Cyclic, differential-pulse, and rotating-disk-electrode voltammetric studies in aqueous solution over the pH range −0.16 to 13.9 reveal seven distinct valence states from [II,II,II] to [IV,V,IV]. The isolated [III,IV,III] complex has acid dissociation constants with pK_a values of 5.0 and 6.8 as determined by glass-electrode titration. Dissociation constants are also reported for other valence states as inferred from the formal reduction potential vs. pH plot. XPS data on the complex reveal peaks at 281.3 and 287.6 eV, which are believed to be due to Ru $3d_{5/2}$ and Ru $3d_{3/2}$ transitions, respectively. The UV–visible spectra of the complex in acidic and basic solutions are presented. In acid, the visible spectrum is dominated by a peak at 649 nm, $\epsilon = 1.04 \times 10^5$ M^{-1} cm^{-1}. The data on the new compound are compared to data on the water oxidation catalyst $[(bpy)_2(OH_2)RuORu(OH_2)(bpy)_2]^{4+}$ and $[(NH_3)_5RuORu(NH_3)_4ORu(NH_3)_5]^{6+}$ (ruthenium red).

Introduction

A remarkable redox chemistry is being uncovered for the aqua and oxo polypyridyl complexes of ruthenium.[1] The monomer $[Ru^{II}(bpy)_2(OH_2)_2]^{2+}$ (bpy = 2,2′-bipyridyl) and the dimer $[(bpy)_2(H_2O)Ru^{III}ORu^{III}(H_2O)(bpy)_2]^{4+}$ each show several higher oxidation states.[2,3] The Ru–bpy dimer (as we will refer to it for

† On leave from the Institute of Physical Chemistry, Polish Academy of Sciences, 01-224 Warsaw, Poland.

(1) Meyer, T. J. *J. Electrochem. Soc.* **1984**, *131*, 221C–228C.

0020-1669/86/1325-2015$01.50/0

convenience) has been found to perform as a redox catalyst for the important oxidations of water to oxygen,[4,5] of chloride to chlorine,[6] and of several organic substrates;[7] however, the mechanisms of these reactions are still unclear.

This report deals with the preparation, characterization, and electrochemical properties of a new bis(μ-oxo)-bridged trimer, $[(bpy)_2(H_2O)RuORu(bpy)_2ORu(H_2O)(bpy)_2]^{6+}$, which can be considered as a third member of a series that includes the monomer and the Ru–bpy dimer. (For convenience, this new species will be referred to as the Ru–bpy trimer.) The complex is of interest as an analogue to the trimeric ammine complex "ruthenium red",[8] which is notable both as a biological stain and for its redox properties. More importantly to us, the reactivity of the Ru–bpy trimer could conceivably shed light on the mechanisms of redox catalysis by the Ru–bpy dimer and suggest the role of the number of metal centers in determining the catalytic properties of complexes of this type.

Experimental Section

Solutions for analytical measurements were prepared by using HPLC grade water. Elemental analyses were performed by Galbraith Laboratories, Knoxville, TN. Trifluoromethanesulfonic acid (HTFMS) was purified by vacuum distillation of the monohydrate.

Preparations. $[Ru(bpy)_2Cl_2]\cdot 2H_2O$ was prepared as previously described.[9]

$[(bpy)_2(H_2O)RuORu(bpy)_2ORu(OH_2)(bpy)_2](ClO_4)_6\cdot 7H_2O$. A solution of 60 mL of water, containing 2.2 g of $[Ru(bpy)_2Cl_2]\cdot 2H_2O$ (4.2 mmol) was stirred and heated to boiling. A silver nitrate solution made by dissolving 1.25 g (5.4 mmol) of silver oxide in a slight excess of dilute nitric acid was added, and the solution was heated at reflux for 30 min. The solution was cooled to room temperature and filtered, and 1 mL of 10% H_2O_2 was added to the filtrate. This solution was evaporated on a hot plate to 50 mL and then filtered, and 15 g of sodium perchlorate was added. The solution was cooled in a refrigerator. The slightly gummy crude product was collected, and the filtrate was saved for recovery of the Ru–bpy dimer (see below). The crude product was recrystallized twice from 80 mL of 1% sodium perchlorate, yielding lustrous red-brown microcrystals, approximately 0.27 g (9%). These were collected and dried in a vacuum desiccator. Anal. Calcd for $[Ru_3(bpy)_6O_2(OH_2)_2](ClO_4)_6\cdot 7H_2O$: C, 35.48; H, 3.28; N, 8.26; Cl, 10.47. Found (average of analyses of two batches): C, 35.33 ± 0.21; H, 3.31 ± 0.15; N, 8.46 ± 0.61; Cl, 8.90 ± 0.51. Fw = 2031. This formula weight was assumed in all stock solution preparations.

$[(bpy)_2(H_2O)RuORu(H_2O)(bpy)_2](ClO_4)_4\cdot 2H_2O$. The filtrate from the collection of the crude product of the Ru–bpy trimer was treated with a small amount of ferrous perchlorate until the solution turned blue, and excess sodium perchlorate was added, precipitating the previously described Ru–bpy dimer.[3,4] This was purified by recrystallization from aqueous sodium perchlorate, yielding approximately 0.59 g (20%).

pH Titrations. Aqueous solutions of the Ru–bpy trimer, approximately 10^{-4} M, were titrated with 0.0100 M sodium hydroxide by using an automatic titrator (Radiometer pHM 62 pH meter, TTT 60 titrator, ABU 11 autoburette, and REC 6 servograph). End points were determined visually, and pK_a values were determined as the pH at 0.5 and 1.5 equiv of base added. The lower pK_a was corrected for the concentration of hydrogen ion.[10] No correction was made for the proximity of the two pK_a's or for activity coefficients.

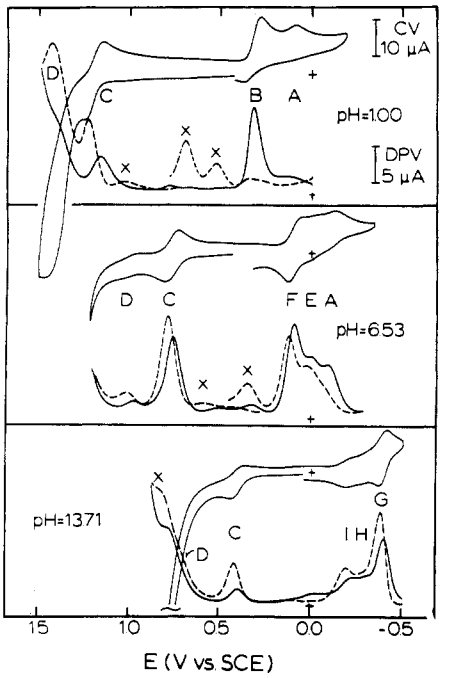

Figure 1. Cyclic (upper, solid line) and differential-pulse (lower) positive (dashed line) and negative (solid line) scan voltammograms of 0.5 mM Ru–bpy trimer at three indicated values of pH, at a glassy-carbon electrode (μ = 0.1 M). The CV potential scan rate was 50 mV/s. The DPV potential scan rate was 5 mV/s, with pulse amplitude of 5 mV. Electrode surface area was 0.0712 cm^2. Waves labeled A through I are intrinsic to the trimer and are discussed in the text. The waves labeled with an × are due to decomposition products, which arise when scans are begun at sufficiently reductive potentials. See text.

Electrochemistry. For cyclic (CV) and differential-pulse (DPV) voltammetry, a PAR Model 174 polarographic analyzer and a signal generator were used, and a glassy-carbon electrode (BAS model MF2012) was the working electrode. The Ru–bpy trimer concentration was ca. 0.5 mM. For electrolytes, trifluoromethanesulfonic acid (HTFMS), ca. 1 M, was used for pH −0.16. NaTFMS/HTFMS solutions were used for pH 1–3, 0.05 M phthalate for pH 3–6, 0.05 M phosphate buffer for pH 6–12.3 and dilute NaOH for pH 12.8–13.9. pH was determined by using a Radiometer pHM62 pH meter and was corrected for sodium ion concentration at high pH. All potentials are referenced to the saturated potassium chloride calomel electrode (SCE).

Bulk electrolysis was performed in a beaker with a VCA carbon cloth (Union Carbide Corp., Danbury, CT) working electrode, SCE reference electrode, and a Pt-wire auxiliary electrode separated by a glass frit. The working solution (10 mL) was 1.7×10^{-4} M Ru–bpy trimer in 0.1 M $HClO_4$. A PAR Model 173 potentiostat and Model 179 digital coulometer were used. Background currents were measured and electrolyses performed at −0.100, 0.350, 0.560 and 0.900 V. The experiment was performed in subdued light.

Two sets of rotating-disk-electrode (RDE) experiments were performed by using a Pine Instruments Co. (Grove City, PA) analytical rotator, and a Model RDE3 potentiostat, in a three-compartment cell, with a Teflon-sheathed glassy-carbon electrode (GC-30, Tokai Carbon, Inc.) of surface area 0.0712 cm^2. Rotation rates ranged from 64 to 10 000 rpm, and the potential was scanned at 10 mV/s. In the first set, performed in pH 9.96 borate (0.01 M) buffer, the potential was scanned from 0.3 to 1.1 V and from +0.2 to −0.5 V. In the second set, performed at pH 13.00 (0.1 M NaOH), the potential was scanned from 0.2 to 0.9 V and from 0.0 to −0.5 V.

X-ray Photoelectron Spectroscopy. XPS data were obtained by using a Perkin-Elmer Physical Electronics Model 548 spectrometer. Solid samples of $[(bpy)_2(H_2O)RuORu(bpy)_2ORu(H_2O)(bpy)_2](ClO_4)_6\cdot 7H_2O$ and $[(bpy)_2(H_2O)RuORu(OH_2)(bpy)_2](ClO_4)_4\cdot 2H_2O$ were pressed onto indium foil. The C 1s peak was assigned the value of 284.6 eV and used as an internal reference.

(2) (a) Takeuchi, K. J.; Samuels, G. J.; Gersten, S. W.; Gilbert, J. A.; Meyer, T. J. *Inorg. Chem.* **1983**, *22*, 1407–1409. (b) Takeuchi, K. J.; Thompson, M. S.; Pipes, D. W.; Meyer, T. J. *Inorg. Chem.* **1984**, *23*, 1845–1851. (c) Che, C.-M.; Wong, K.-Y.; Leung, W.-H.; Poon, C.-K. *Inorg. Chem.* **1986**, *25*, 345–348.
(3) Gilbert, J. A.; Eggleston, D. S.; Murphy, W. R., Jr.; Geselowitz, D. A.; Gersten, S. W.; Hodgson, D. G.; Meyer, T. J. *J. Am. Chem. Soc.* **1985**, *107*, 3855–3864.
(4) Gersten, S. W.; Samuels, G. J.; Meyer, T. J. *J. Am. Chem. Soc.* **1982**, *104*, 4029–4030.
(5) (a) Honda, K.; Frank, A. J. *J. Chem. Soc., Chem. Commun.* **1984**, 1635–1636. (b) Collin, J. P.; Sauvage, J. P. *Inorg. Chem.* **1986**, *25*, 135–146.
(6) (a) Ellis, C. D.; Gilbert, J. A.; Murphy, W. R., Jr.; Meyer, T. J. *J. Am. Chem. Soc.* **1983**, *105*, 4842–4843. (b) Vining, W. J.; Meyer, T. J. *Inorg. Chem.*, following paper in this issue; *J. Electroanal. Chem. Interfacial Electrochem.* **1986**, *195*, 183–187.
(7) (a) Kutner, W.; Gilbert, J. A.; Murray, R. W.; Meyer, T. J. *J. Electroanal. Chem. Interfacial Electrochem.*, in press. (b) Kutner, W.; Meyer, T. J.; Murray, R. W. *J. Electroanal. Chem. Interfacial Electrochem.* **1985**, *195*, 375–394.
(8) Mathieson, A. McL.; Mellon, D. P.; Stephenson, N. C. *Acta Crystallogr.* **1952**, *5*, 185–186.
(9) Sullivan, B. P.; Salmon, D. J.; Meyer, T. J. *Inorg. Chem.* **1978**, *17*, 3334–3341.
(10) Albert, A.; Sarjeant, E. P. *The Determination of Ionization Constants: A Laboratory Manual*, 3rd ed., Chapman and Hall: London, 1983, p 27.

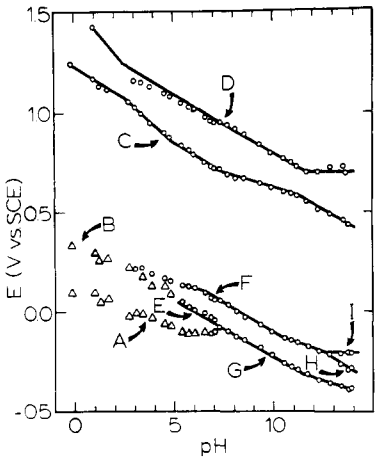

Figure 2. Dependence of formal reduction potentials of Ru–bpy trimer couples on pH (μ = 0.1 M; Results).

Results

pH Titration. Titration of the Ru–bpy trimer with sodium hydroxide reveals two acid dissociation steps, assigned to the acid dissociation equilibria

$$[(bpy)_2(H_2O)Ru^{III}ORu^{IV}(bpy)_2ORu^{III}(OH_2)(bpy)_2]^{6+} \rightleftharpoons [(bpy)_2(HO)Ru^{III}ORu^{IV}(bpy)_2ORu^{III}(OH_2)(bpy)_2]^{5+} + H^+ \quad (1)$$

$$[(bpy)_2(HO)Ru^{III}ORu^{IV}(bpy)_2ORu^{III}(OH_2)(bpy)_2]^{5+} \rightleftharpoons [(bpy)_2(HO)Ru^{III}ORu^{IV}(bpy)_2ORu^{III}(OH)(bpy)_2]^{4+} + H^+ \quad (2)$$

The pK_a values for the two steps are 5.0 ± 0.1 and 6.8 ± 0.1, respectively. The formula weight of the compound was found to be approximately 2000.

Electrochemistry. Cyclic voltammograms of the Ru–bpy trimer in acidic, neutral, and basic solutions are shown in Figure 1. The relationships between the formal or peak potentials and pH for the observed couples are shown in Figure 2. For the well-defined cyclic voltammograms (CV), the averages of the cathodic and anodic peak potentials from cyclic voltammetry or the average of peak potentials on positive and negative scan direction from differential pulse voltammetry (DPV) are indicated by circles. Closely spaced peaks were deconvoluted manually. For the ill-defined CV's (weak or absent anodic CV or DPV peaks), the negative scan DPV peak potentials are plotted as triangles.

At low pH, four distinct redox couples are seen (labeled A–D in Figures 1 and 2). As the pH is raised, the couples generally shift to more negative potentials. At pH >3, couple B separates into two couples, E and F. At pH >6.5, couples E and A merge to give couple G. At pH >13, peak F splits to give peaks H and I.

The curves in Figure 2 are drawn to fit the data to straight-line segments with slopes of −30, −60, −90, or −120 mV/pH unit. These correspond to the theoretical values for proton-accompanied electron transfer for processes of $2e^- + 1H^+$, $2e^- + 2H^+$ or $1e^- + 1H^+$, $2e^- + 3H^+$, and $1e^- + 2H^+$, respectively. For processes A, B, and E, in acidic solution no lines were constructed because of the irreversible nature of the couples. Under these conditions the trimer is irreversibly reduced, decomposing to the component monomers. Line D shows a slope of −120 for pH $\lesssim$2.0 and a slope of −60 mV/pH for 2.0 < pH $\lesssim$ 11.5 and is pH-independent for pH $\gtrsim$11.5. Process D is nearly electrochemically reversible in the region 8.0 $\lesssim$ pH $\lesssim$ 11.0. Reversibility and wave shape deteriorate at high and low pH. Line C shows a slope of −60 for pH <3.0, −90 for 3.0 $\lesssim$ pH $\lesssim$ 4.5, −60 for 4.5 $\lesssim$ pH < 7.0, −30 for 7.0 $\lesssim$ pH $\lesssim$ 11.0, and −60 for pH $\gtrsim$11.0. Line F shows a slope of −60 for 6.8 < pH $\lesssim$ 10.8 and −30 for 10.8 $\lesssim$ pH $\lesssim$ 12.5. The slope of line I is zero, while that of H has a slope of −60. Line G shows a slope of −60 for pH $\lesssim$11.8 and −30 at pH $\gtrsim$11.8.

Small peaks were occasionally found in the potential region between couples F and C when the potential was scanned by starting from values more positive than $E°$ of couple D. We attribute these peaks to decomposition products of Ru–bpy trimer and they are labeled with an × in Figure 1.

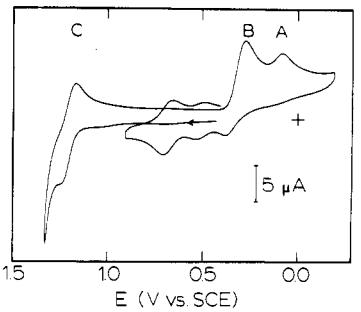

Figure 3. Cyclic voltammogram of 0.5 mM Ru–bpy trimer at a glassy-carbon electrode, pH 1.0 (HTFMS). The potential scan rate was 100 mV/s. The starting point is near the arrow, which indicates initial scan direction. Electrode surface area was 0.0712 cm^2.

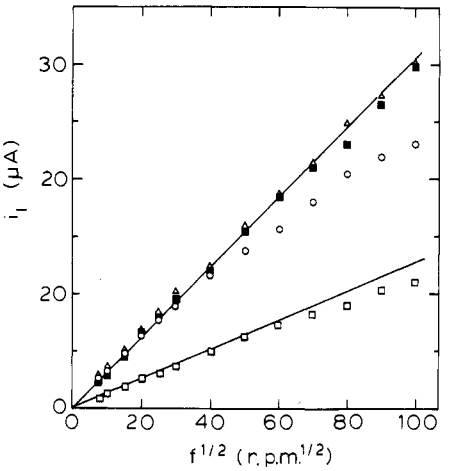

Figure 4. RDE limiting current vs. the square root of rotation rate at a glassy-carbon electrode for 0.265 mM Ru–bpy trimer at pH 9.96. Data are shown for couples of $E_{1/2}$ at (○) 0.62 (wave C), (□) 0.78 (wave D), (▲) −0.12 (wave F), and (■) −0.25 (wave G) V. Electrode surface area was 0.0712 cm^2 (μ = 0.1 M).

Cyclic voltammetry of the Ru–bpy trimer at pH 1.00 (0.10 M HTFMS) reveals irreversible reduction peaks B and A at 0.27 and 0.07 V, followed by the appearance upon reversal of sweep direction at −0.2 V (i.e., at a potential more negative than the cathodic peak, A) of reversible couples at $E_{1/2}$ = 0.66 and 0.49 V, as shown in Figure 3. This behavior is attributed to the hydrolysis of the Ru–bpy trimer, upon reduction to the Ru(II) form, to give a mixture of cis and trans isomers of $[Ru(bpy)_2(OH_2)_2]^{2+}$.[2] The ratio of the anodic peak heights was roughly 2:1 for the couples at $E_{1/2}$ = 0.66 and 0.49 V.

Bulk electrolytic reduction of the Ru–bpy trimer in 0.1 M $HClO_4$ with the potential held at −0.100 V occurred with the transfer of 3.9 ± 0.15 equiv/mol. Oxidation of the resulting solution at 0.560 V (halfway between the formal potentials of *trans*- and *cis*-$[Ru(bpy)_2(OH_2)_2]^{3+/2+}$) occurred with n = 1.0 ± 0.1, and subsequent oxidation at 0.900 V involved approximately 2.0 equiv/mol. These data indicate that the Ru–bpy trimer molecule is reduced by four electrons to yield one *trans*- and two *cis*-$[Ru(bpy)_2(OH_2)_2]^{2+}$ molecules.

The RDE experiments were performed on samples of the Ru–bpy trimer at 2.65 × 10^{-4} M. At pH 9.96, two steps in the positive scan at $E_{1/2}$ = 0.62 and 0.78 V and two steps in the negative scan at −0.12 and −0.25 V were recorded. The $E_{1/2}$ values are consistent with the formal redox potentials of couples C, D, F, and G, respectively, obtained by cyclic voltammetry (Figure 2). The limiting currents, i_l, for the four steps were measured at 0.69, 0.90, −0.19 and −0.40 V, respectively, and were corrected for background currents measured in buffer alone. Levich plots for the four steps are shown in Figure 4. The data for processes F and G fall on reasonably straight lines, both of slope 0.124 μA/min$^{1/2}$. The data

Table I. Diffusion Coefficients for the Ru–bpy Trimer and Related Species Determined from RDE Data

species	10^6D, $cm^2\ s^{-1}$
$[(bpy)_2(HO)Ru^{IV}ORu^{IV}(bpy)_2ORu^{IV}(O)(bpy)_2]^{5+}$	2.0[a]
$[(bpy)_2(HO)Ru^{III}ORu^{IV}(bpy)_2ORu^{III}(OH)(bpy)_2]^{4+}$	2.8,[a] 3.1[b]
$[(bpy)_2(H_2O)Ru^{II}ORu^{IV}(bpy)_2ORu^{II}(OH_2)(bpy)_2]^{4+}$	2.8[a]
$[(bpy)_2(HO)Ru^{II}ORu^{IV}(bpy)_2ORu^{II}(OH_2)(bpy)_2]^{3+}$	3.6
$[(bpy)_2(HO)Ru^{III}ORu^{III}(OH)(bpy)_2]^{2+}$	3.7,[c,b] 2.2[c,d]
$[(tpy)(phen)Ru^{II}(OH)]^{+}$	4.6[b,e]

[a] pH 9.96 (0.01 M borate buffer). [b] pH 13.00 (0.10 M NaOH). [c] Reference 7a. [d] pH 13.00–14.00 (1.0 M KNO_3). [e] Reference 7b.

for processes C and D both lie on straight lines at lower rotation rates, f, but fall below the lines at higher rotation rates. The observed curvature may be due to the onset of kinetic limitation to the redox process at higher rotation rates.[11] The slopes of the straight portions are 0.124 and 0.050 $\mu A/min^{1/2}$ for C and D, respectively. Since the slope for the straight portion of line D is approximately half of those of F, G, and C, we assign D as a one-electron process and F, G, and C as two-electron processes, assuming similar diffusion coefficients for the various oxidation states of the Ru–bpy trimer.

Logarithmic analysis of RDE curves (E vs. log $[(i_l - i)/i]$) of the four steps at $f = 900$ rpm, which is in the straight portion of the Levich plots, gave straight lines with slopes of 40, 90, 37, and 37 mV for processes C, D, F, and G, respectively. The slopes of 40 and 90 mV are sufficiently close to the theoretical values of 30 and 60 mV expected for two- and one-electron processes to support the conclusions reached from the Levich plots.

From the data acquired at pH 9.96, processes C and F are assigned to oxidation and reduction of $[(bpy)_2(HO)Ru^{III}ORu^{IV}(bpy)_2ORu^{III}(OH)(bpy)_2]^{4+}$, respectively. Process D is an oxidation of $[(bpy)_2(HO)Ru^{IV}ORu^{IV}(bpy)_2ORu^{IV}(O)(bpy)_2]^{5+}$, and process G is a reduction of $[(bpy)_2(H_2O)Ru^{II}ORu^{IV}(bpy)_2ORu^{II}(OH_2)(bpy)_2]^{4+}$. The proton compositions of the oxidized and reduced species are discussed in a later section. Diffusion coefficients calculated from the slopes of the Levich plots by using the assigned value of n and 0.010 $cm^2\ s^{-1}$ as the kinematic viscosity of pure water are shown in Table I.

At pH 13.00 (0.10 M NaOH), two steps in the negative scan at –0.21 and –0.37 V, and one in the positive scan at 0.49 V, are observed, consistent with the formal potentials of redox couples F, G, and C, respectively, as obtained by cyclic voltammetry (Figure 2). The step corresponding to process D is very ill-defined and occurs at $E_{1/2} = 0.73$ V and is superimposed on a large background current. Curiously, the background current is smaller than the background measured in the absence of Ru–bpy trimer, which prevented any attempt to subtract the independently measured background from the observed current. The limiting currents for steps C, F, and G were measured at 0.560, 0.275, and –0.425 V, respectively, and were corrected for background currents measured in 0.100 M NaOH alone.

The data for process C at $E_{1/2} = 0.49$ V fall on a straight line, while the data for steps F and G show a slight curvature. The slopes of the lines of the Levich plot are 0.132, 0.132, and 0.146 $\mu A/min^{1/2}$ for the processes with $E_{1/2} = 0.49$, –0.21, and –0.37 V, respectively.

Logarithmic analyses for processes C, F, and G at $f = 900$ rpm resulted in straight lines with slopes of 55, 55, and 33 mV, respectively. The higher than predicted slopes for processes F and C might indicate that two closely spaced one-electron processes are being observed at this pH rather than a two-electron process. For F, this is consistent with Figure 2, which shows that at slightly higher pH values, couple F splits into couples H and I.

At pH 13 processes C and F at $E_{1/2} = 0.49$ and –0.21 V arise from oxidation and reduction of $[(bpy)_2(HO)Ru^{III}ORu^{IV}(bpy)_2ORu^{III}(OH)(bpy)_2]^{4+}$, however, because of changes in proton content for the oxidized and reduced species, process G at $E_{1/2} = -0.37$ V corresponds to reduction of $[(bpy)_2(HO)Ru^{II}ORu^{IV}(bpy)_2ORu^{II}(OH_2)(bpy)_2]^{3+}$ (see Discussion). Values of $n = 2$ for each process (see Discussion) and 0.0102 $cm^2\ s^{-1}$ as the kinematic viscosity[12] of 0.1 M NaOH were used in the Levich equation to calculate diffusion coefficients (Table I). Diffusion coefficients for the dimer $[(bpy)_2OHRuORuOH(bpy)_2]^{2+}$ and monomer $[Ru(tpy)(phen)OH]^{+}$ (tpy is 2,2′,2″-terpyridine)[7] are also included for purposes of comparison.

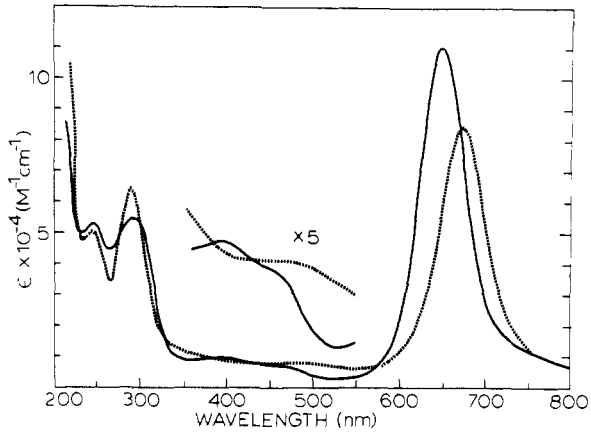

Figure 5. Ultraviolet–visible spectra of 1.22×10^{-5} M Ru–bpy trimer in 0.1 M HTFMS (solid line) and 0.1 M NaOH (dashed line).

Table II. UV–Visible Spectral Data for the Ru–bpy Trimer and Related Species

species	λ_{max}, nm	ϵ,[e] M^{-1} cm^{-1}
$[(bpy)_2(OH_2)RuORu(bpy)_2ORu(OH_2)(bpy)_2]^{6+}$ [a]	653	105 000
	462 (sh)	7 200
	393	9 990
	295	54 000
	277 (sh)	48 900
	246	52 100
$[(bpy)_2(OH)RuORu(bpy)_2ORu(OH)(bpy)_2]^{4+}$ [b]	673	80 400
	475 (sh)	7 800
	353 (sh)	10 900
	288	62 500
	246	50 200
$[(bpy)_2(OH_2)RuORu(OH)_2(bpy)_2]^{4+}$ [a,c]	637	21 100
	280	50 300
	271	39 800
$[(bpy)_2(OH)RuORu(OH)(bpy)_2]^{2+}$ [b,d]	623	
$[(NH_3)_5RuORu(NH_3)_4ORu(NH_3)_5]^{6+}$ [c]	758	1 000
	532	69 900
	375	6 300
	245	6 000
$[(NH_3)_5RuORu(NH_3)_5]^{4+}$ [f]	504	16 230
	386	5 430

[a] In 0.1 M HTFMS. [b] In 0.1 M NaOH. [c] Reference 8. [d] Reference 3. [e] ±5%. [f] In CH_3CN. Baumann, J. A.; Meyer, T. J. *Inorg. Chem.* **1980**, *19*, 345–350.

UV–Visible Spectra. Spectra of the Ru–bpy trimer in acidic and basic aqueous solutions are shown in Figure 5. The visible spectrum of the diaqua form in 0.1 M HTFMS (Figure 5) is dominated by an intense band at 653 nm, which shifts to 674 nm upon deprotonation to the dihydroxo form in 0.1 M NaOH. Two smaller bands in the 350–500-nm region also shift upon deprotonation. Data on the spectral features are summarized in Table II.

X-ray Photoelectron Spectra. The X-ray photoelectron spectra of $[(bpy)_2(H_2O)Ru^{III}ORu^{IV}(bpy)_2ORu^{III}(OH_2)(bpy)_2](ClO_4)_6 \cdot 7H_2O$ and $[(bpy)_2(H_2O)Ru^{III}ORu^{III}(OH_2)(bpy)_2](ClO_4)_4 \cdot 2H_2O$ in the region 276–294 eV include peaks at 281.3 and 281.1 eV for the Ru–bpy trimer and Ru–bpy dimer, respectively, which can be assigned as Ru $3d_{5/2}$ peaks. A peak at 287.6 eV in the Ru–bpy trimer spectrum can be assigned as a Ru

(11) Bard, A. J.; Faulkner, L. R. *Electrochemical Methods*; Wiley: New York, 1980; p 291.

(12) Weast, R. C., Ed. *CRC Handbook of Chemistry and Physics*, 63rd ed.; CRC Press: Boca Raton, FL, 1983; p D-265.

$3d_{3/2}$ peak. Unfortunately, it is impossible to resolve other peaks lying under the large C 1s peak at 284.6 eV in either spectrum.

On the basis of the relative areas of the XPS peaks for chlorine, nitrogen, and oxygen, and from published sensitivity factors,[13] the atom ratios for the XPS samples can be determined. For the Ru–bpy trimer, a Cl:N:O atom ratio of 1:1.85:5.09 was determined. The calculated ratio for the complex salt as the trihydrate is 1:2.0:5.16. For the Ru–bpy dimer, a ratio of 1:1.67:5.30 was obtained experimentally, and the calculated ratio for the complex salt as the dihydrate is 1:2.0:5.25.

Discussion

Characterization of the Trimer. After repeated attempts we have been unable to obtain crystals of the trimer suitable for X-ray structural analysis. However, the available evidence is strongly supportive of a trimer formulation. In particular, bulk electrolysis and CV experiments show that the molecule is reduced by four electrons to give one *trans*- and two cis-$[Ru^{II}(bpy)_2(OH_2)_2]^{2+}$ molecules. Earlier work[3] has shown that two-electron reduction of the Ru(III)–Ru(III) dimer $[(bpy)_2(H_2O)RuORu(H_2O)(bpy)_2]^{4+}$ leads to two molecules of *cis*-$[Ru^{II}(bpy)_2(OH_2)_2]^{2+}$.[3] The trimer formulation is consistent with the elemental analysis data and with equivalent weight estimates based on pH titration and coulometry. The available evidence strongly suggests that the two end sites are chemically equivalent, and given the production of one *trans*- and two *cis*-$[Ru(bpy)_2(H_2O)_2]^{2+}$ products upon reduction, the most likely formulation is as the cis–trans–cis trimer bis[(μ-oxo)-*cis*-aqua[bis(2,2′-bipyridine)ruthenium(III)]-*trans*-bis(2,2′-bipyridine)ruthenium(IV)(6+) cation

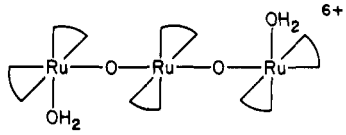

where the arcs represent chelating 2,2′-bipyridine ligands. Although the *trans*-bis(bipyridyl) structure at Ru is uncommon, it has been reached by photochemical and thermal routes.[14] The cis configuration has been established crystallographically for the Ru(III) sites in the dimer $[(bpy)_2(H_2O)RuORu(H_2O)(bpy)_2]^{4+}$.[3]

Given the possibility of strong electronic coupling among the Ru sites through the oxo groups, the description of oxidation states as Ru(III)–Ru(IV)–Ru(III) is clearly somewhat arbitrary but the XPS spectrum is consistent with the presence of chemically different sites. The evidence is the appearance of the Ru $3d_{5/2}$ component of the $3d_{5/2}$,$3d_{3/2}$ doublet at 281.3 eV and the appearance of the $3d_{3/2}$ component for the second site at 287.6 eV. This result might have been expected anyway given the structurally distinct nature of the central Ru.

From the electrochemical results it follows that the trimer has seven redox states accessible. The sum of oxidation states at the individual Ru sites ranges from 6 to 13 (with 11 missing) through the seven trimer states. We have assigned formal oxidation states to the three ruthenium sites in the complex on the basis of the following assumptions: (1) the two end ruthenium sites have the same formal oxidation state, and (2) the central ruthenium site has a valence greater than or equal to the oxidation state at the end ruthenium sites. In our designation the seven redox states of the trimer are thus [II,II,II], [II,III,II], [II,IV,II], [III,III,III], [III,IV,III], [IV,IV,IV], and [IV,V,IV]. Other designations are possible, e.g. [II,III,III] rather than [II,IV,II]. In addition, all such designations assume a "localized" description of oxidation states. In fact, there is evidence for electronic delocalization between sites in the trimer from (1) the appearance of the intense, visible transition for the [III,IV,III] trimer, which, given its molar extinction coefficient, is probably a transition between delocalized molecular levels, and (2) the unusually low Ru(III) binding energy for the [III,IV,III] trimer as discussed below. In any given case, if electronic delocalization effects are sufficiently large, a delocalized description, e.g., $[III^1/_3,III^1/_3,III^1/_3]$, may be more appropriate than a localized description, [III,IV,III]. In the absence of evidence on this point, we will use the localized labels for convenience.

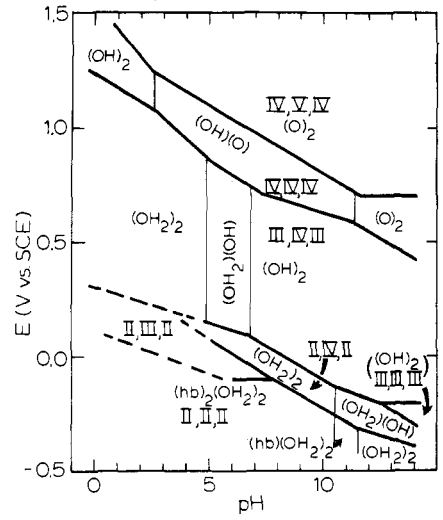

Figure 6. Pourbaix (pH vs. formal potential) diagram for the various trimeric couples derived from the data in Figure 2 (μ = 0.1 M). The vertical lines are at the pK_a values for the redox states of the trimer indicated (see text). Formal oxidation states at the individual redox sites using the designations described in the text are indicated by roman numeral triplets. The proton compositions at the aquo groups of the terminal Ru sites are indicated by, for example, $(OH)_2$–III,IV,III for $[(bpy)_2(OH)Ru^{III}ORu^{IV}(bpy)_2ORu^{III}(OH)(bpy)_2]^{2+}$. The abbreviation (hb) is used to indicate protonation at an oxo bridge to give an hydroxo bridge, e.g. $(hb)(OH_2)_2$–II,II,II for $[(bpy)_2(OH_2)Ru^{II}(OH)Ru^{II}(bpy)_2ORu^{II}(OH_2)(bpy)_2]^{3+}$. The dashed lines are extrapolations based on peak potentials from differential-pulse voltammetry data obtained under conditions where the couples are chemically irreversible.

Our suggestion of oxidation state (Ru(III)–Ru(IV)–Ru(III)) and trans geometry at the central Ru site in the Ru–bpy trimer

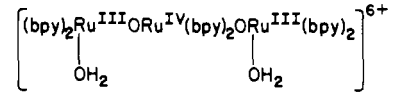

are consistent with the known structure of ruthenium red,[8] $[(NH_3)_5Ru^{III}ORu^{IV}(NH_3)_4ORu^{III}(NH_3)_5]^{6+}$. In principle, the Ru–bpy trimer can exist in three diastereomeric forms: the enantiomeric pair with either Δ or Λ configuration at the terminal Ru sites or the meso form with one Δ and one Λ terminal site. We have no evidence as to the distribution of possible isomers in the isolated compound.

Redox Chemistry. The Ru–bpy trimer is remarkable in that it can exist in seven distinct redox states as revealed by the electrochemical studies. The redox potential–pH characteristics of couples involving the various oxidation states can be discerned from the Pourbaix diagram in Figure 6, which was constructed from the data in Figure 2. The redox characteristics of the system are complicated by the fact that each of the trimer oxidation states has its own acid–base equilibria at the two aqua ligands and/or at the two oxo bridges. As discussed below, the proton and electron compositions of the components of the various couples follow from the pH-dependent electrochemical studies. The pH–potential variations in Figure 6 show how the formal potential for a redox couple varies with pH. The vertical lines are pK_a values for the various redox states of the trimer as indicated.

In the areas of the diagram labeled with regard to oxidation state and proton content, the redox potential and pH are such that

(13) Wagner, D.; Davis, L. E.; Zeller, M. V.; Taylor, J. A.; Raymond, A. H.; Gale, L. H. *SIA, Surf. Interface Anal.* **1981**, *3*, 211–225.

(14) (a) Durham, B.; Wilson, S. R.; Hodgson, D. J.; Meyer, T. J. *J. Am. Chem. Soc.* **1980**, *102*, 600–607. (b) Walsh, J. L.; Durham, B. *Inorg. Chem.* **1982**, *21*, 329–332. (c) Cordes, A. W.; Durham, B.; Swepston, P. N.; Pennington, W. T.; Condren, S. M.; Jensen, R.; Walsh, J. L. *J. Coord. Chem.* **1982**, *11*, 251–260. (d) Bonneson, P.; Walsh, J. L.; Pennington, W. T.; Cordes, A. W.; Durham, B. *Inorg. Chem.* **1983**, *22*, 1761–1765.

a single redox state of the trimer is the dominant form. For example, in the pH–potential area labeled (OH)(O)–IV,IV,IV, the dominant form of the trimer is $[(bpy)_2(O)Ru^{IV}ORu^{IV}(bpy)_2ORu^{IV}(OH)(bpy)_2]^{5+}$. The bases for the assumptions with regard to proton content and oxidation state are discussed below.

Oxidation States and Proton Content. For the processes in Figure 2, the couples labeled C, F, and G involve net two-electron changes for the following reasons: (1) The slopes of Levich plots from RDE experiments at pH 9.96 are nearly the same. (2) Bulk electrolysis of the starting Ru(III)–Ru(IV)–Ru(III) trimer below couples F and G involves four electrons to give two *cis*- and one *trans*-$[Ru^{II}(bpy)_2(H_2O)_2]^{2+}$. (3) There are segments in the pH–potential diagram where slopes of −30 and −90 mV/pH unit are observed, which are consistent with two-electron–one-proton and two-electron–three-proton processes, respectively. In strongly basic solution, couple F splits into two one-electron couples H and I. Couple D is a one-electron couple from the Levich plots in Figure 4.

From the known proton and electron composition of the isolated and characterized [III,IV,III] trimer and the pH dependences and numbers of electrons involved for the processes in Figure 2, it is possible to infer the electron and proton contents of the various forms of the trimer. The evidence available from the pH-dependent electrochemical studies will be considered in turn.

1. Reduction of the [III,IV,III] State. Above pH 6.8, [III,IV,III] exists as $[(bpy)_2(OH)Ru^{III}ORu^{IV}(bpy)_2ORu^{III}(OH)(bpy)_2]^{4+}$ from the pH titrations. From pH 6.8–10.7 [III,IV,III] undergoes a two-electron–two-proton reduction to [II,IV,II], presumably $[(bpy)_2(H_2O)Ru^{II}ORu^{IV}(bpy)_2ORu^{II}(H_2O)(bpy)_2]^{4+}$. The increase in proton content upon reduction favors the designation [II,IV,II] over [III,II,III] for the reduced species. From pH 10.7–12.5, the slope of the E vs. pH plot changes to −30 mV/pH, implying a change to a two-electron–one-proton process and reduction to $[(bpy)_2(OH)Ru^{II}ORu^{IV}(bpy)_2ORu^{II}(OH_2)(bpy)_2]^{3+}$. From the break in the E vs. pH plot, pK_{a1} for [II,IV,II] can be estimated to be 10.7. At pH 12.5, the two-electron reduction splits into two one-electron reductions. The first reduction (line I) is pH-independent to give $[(bpy)_2(OH)Ru^{III}ORu^{III}(bpy)_2ORu^{III}(OH)(bpy)_2]^{3+}$ and the second (line H) is a one-electron–one-proton reduction to give $[(bpy)_2(OH)Ru^{II}ORu^{IV}(bpy)_2ORu^{II}(H_2O)(bpy)_2]^{3+}$ (eq 3 and 4). The assignment of the one-electron-reduced trimer as [III,III,III] is consistent with our scheme for designating oxidation states, but an equally valid possibility is the triple mixed-valence ion [II,IV,III].

$$[(bpy)_2(OH)Ru^{III}ORu^{IV}(bpy)_2ORu^{III}(OH)(bpy)_2]^{4+} + e^- \rightarrow [(bpy)_2(OH)Ru^{III}ORu^{III}(bpy)_2ORu^{III}(OH)(bpy)_2]^{3+} \quad (3)$$

$$[(bpy)_2(OH)Ru^{III}ORu^{III}(bpy)_2ORu^{III}(OH)(bpy)_2]^{3+} + e^- + H^+ \rightarrow [(bpy)_2(OH)Ru^{II}ORu^{IV}(bpy)_2ORu^{II}(OH_2)(bpy)_2]^{3+} \quad (4)$$

There is precedence for the pH-induced splitting of a two-electron couple into two one-electron couples, in related monomeric couples.[2,15] For example, the Ru(IV)/Ru(III) and Ru(III)/Ru(II) couples associated with $[Ru(bpy)_2(py)(H_2O)]^{2+}$ over the pH range 2 to 10 are[2b]

$$[(bpy)_2(py)Ru^{IV}(O)]^{2+} + e^- + H^+ \rightarrow [(bpy)_2(py)Ru^{III}(OH)]^{2+} \quad (5)$$

$$[(bpy)_2(py)Ru^{III}(OH)]^{2+} + e^- + H^+ \rightarrow [(bpy)_2(py)Ru^{II}(OH_2)]^{2+} \quad (6)$$

However, above pK_{a1} for $[(bpy)_2(py)Ru^{II}(OH_2)]^{2+}$ at pH 10, the Ru(III)/Ru(II) couple becomes pH-independent:

$$[(bpy)_2(py)Ru^{III}(OH)]^{2+} + e^- \rightarrow [(bpy)_2(py)Ru^{II}(OH)]^+ \quad (6a)$$

By pH 11 the potentials for the two couples are the same, Ru(III) becomes unstable with respect to disproportionation, and only the two-electron, Ru(IV)/(II) couple is observed:

$$[(bpy)_2(py)Ru^{IV}(O)]^{2+} + 2e^- + H^+ \rightarrow [(bpy)_2(py)Ru^{II}(OH)]^+ \quad (7)$$

Above pH 11 $[(bpy)_2(py)Ru^{III}(OH)]^{2+}$ is a stronger one-electron oxidant than $[(bpy)_2(py)Ru^{IV}(O)]^{2+}$ because of the difference in proton demands for the Ru(III)/Ru(II) and Ru(IV)/Ru(III) couples. In contrast to the monomer, for the Ru–bpy trimer at pH <12.5, the two-electron nature of the reduction of [III,IV,III] shows that the intermediate oxidation state, [III,II-I,III] is unstable with respect to disproportionation, as inferred from Figure 6. The cause is the same. In solutions more acidic than pH 12.5 [III,III,III] is a stronger oxidant than [III,IV,III] because of the differences in proton content for the [III,IV,-III]/[III,III,III] and [III,III,III]/[II,IV,II] couples in eq 3 and 4. However, the situation is the inverse of that for $[(bpy)_2(py)Ru^{IV}O]^{2+}$ in that loss of a proton from the intermediate oxidation state, [III,III,III], leads to a proton-independent [III,IV,III]/[III,III,III] couple, above pH 12.5. For the monomer a proton is lost from the lowest oxidation state, $[(bpy)_2(py)Ru^{II}(OH_2)]^{2+}$. As for the monomer, the apparent stabilization of the intermediate oxidation state at high pH has its origin in the acid–base characteristics of the three oxidation states involved.

At pH 6.8 the second dissociation constant, pK_{a2} for [III,IV,III] is reached and the couple becomes two-electron two-proton in nature:

$$\left[\begin{matrix} Ru^{III}ORu^{IV}ORu^{III} \\ | \qquad\quad | \\ OH \qquad\quad OH \end{matrix}\right]^{5+} + 2e^- + 2H^+ \longrightarrow \left[\begin{matrix} Ru^{II}ORu^{IV}ORu^{II} \\ | \qquad\quad | \\ OH_2 \qquad\quad OH_2 \end{matrix}\right]^{4+} \quad (8)$$

In eq 8 and later equations, the bpy ligands are omitted for clarity.

At pH 5.0 pK_{a1} is reached, and the dominant form of the [III,IV,III] trimer at pH <5.0 is $[(bpy)_2(H_2O)Ru^{III}ORu^{IV}(bpy)_2ORu^{III}(H_2O)(bpy)_2]^{6+}$. However, the couple is chemically irreversible in solutions this acidic due to hydrolysis of the reduced form of the couple, and the potential data cannot be used for making thermodynamic arguments.

2. Reduction of the [II,IV,II] State. The data in Figure 6 provide evidence for a further two-electron reduction of the [II,IV,II] state. Above pH 7.5, the process (Figure 2, line G) is chemically and electrochemically reversible, showing that the reduced form remains intact at least on the cyclic voltammetry time scale used.

The second two-electron reduction of the [III,IV,III] trimer occurs, at least in a formal sense, at the central ruthenium, [II,IV,II] + 2e⁻ → [II,II,II]. From pH 7–10.5 the slope of −60 mV/pH unit shows that the couple involves the gain of two electrons and two protons:

$$\left[\begin{matrix} Ru^{II}ORu^{IV}ORu^{II} \\ | \qquad\quad | \\ OH_2 \qquad\quad OH_2 \end{matrix}\right]^{4+} + 2e^- + 2H^+ \longrightarrow \left[\begin{matrix} \quad H \quad H \quad \\ Ru^{II}ORu^{II}ORu^{II} \\ | \qquad\quad | \\ OH_2 \qquad\quad OH_2 \end{matrix}\right]^{4+} \quad (9)$$

The only reasonable sites in the trimer that remain to be protonated are the bridging oxo groups, which make bridging hydroxo groups as suggested in eq 9. From the Pourbaix diagram in Figure 6, above pH 10.7, the [II,IV,II] form of the trimer is predominantly in the aqua hydroxo form (see above). Nonetheless, between pH 10.7 and 11.5, the slope of the E vs. pH plot for the

(15) Roecker, L.; Kutner, W.; Gilbert, J. A.; Simmons, M.; Murray, R. W.; Meyer, T. J. *Inorg. Chem.* **1985**, *24*, 3784–3791.

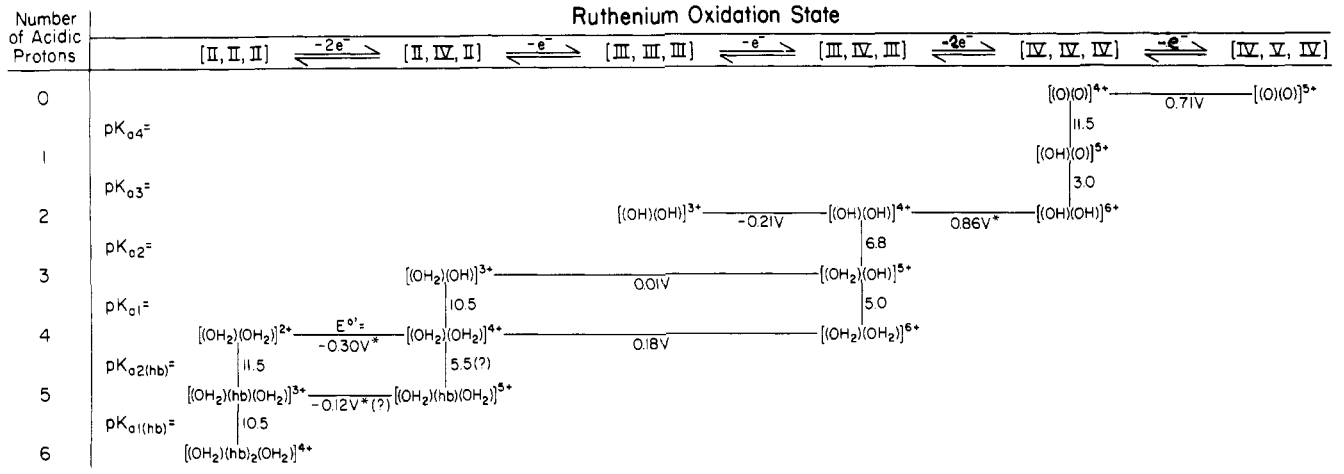

Figure 7. Acid–base (vertical) and redox (horizontal) equilibria for the species $[(bpy)_2(L)RuORu(bpy)_2ORu(L')(bpy)_2]^{n+}$ (μ = 0.1 M). L and L' ligands only are indicated; hb refers to a μ-hydroxo-bridge form. Potentials indicated by asterisks are obtained by extrapolation using pK_a values and theoretical slopes in Figure 6.

[II,IV,II]/[II,II,II] couple remains −60 mV/pH unit. In this pH region the couple must become

$$\left[Ru^{II}ORu^{IV}ORu^{II}(OH_2)(OH)\right]^{3+} + 2e^- + 2H^+ \longrightarrow \left[Ru^{II}HORu^{II}ORu^{II}(OH_2)(OH_2)\right]^{3+} \quad (10)$$

With this interpretation p$K_{a(hb1)}$ for gain and loss of the oxo proton in $[(bpy)_2(OH_2)Ru^{II}(OH)Ru^{II}(bpy)_2(O)Ru^{II}(OH_2)(bpy)_2]^{3+}$ must nearly coincide with pK_{a1} for $[(bpy)_2(OH_2)Ru^{II}(O)Ru^{IV}(bpy)_2(O)Ru^{II}(OH_2)(bpy)_2]^{4+}$. The subscript "hb" refers to the hydroxo-bridge proton.

The change in slope to −30 mV/pH unit at pH >11.5 points to mono protonation of the [II,II,II] trimer and the couple

$$\left[Ru^{II}ORu^{IV}ORu^{II}(OH_2)(OH)\right]^{3+} + 2e^- + H^+ \longrightarrow \left[Ru^{II}ORu^{II}ORu^{II}(OH_2)(OH_2)\right]^{2+} \quad (11)$$

implying that p$K_{a(hb2)}$ for [II,II,II] is 11.5.

If we switch our attention to the region pH <6.8, the complexity of the electrochemical behavior leads to difficulty in interpretation of the proton content of the reduced species. Presumably, the complexity arises at least partly from the hydrolysis reaction following reduction (see Figure 3). We believe that, below pH 5.5, the [II,IV,II] complex may exist in a monohydroxy-bridged form.

3. Two-Electron Oxidation of the [III,IV,III] State. The [III,IV,III] trimer undergoes a two-electron oxidation with the complex pH dependence shown on the Pourbaix diagram (Figure 6). Starting in the most acidic region, from the −60 mV/pH unit slope at pH <3.0 and on the basis of the fact that the [III,IV,III] trimer is the diaqua ion, the oxidation must involve

$$\left[Ru^{III}ORu^{IV}ORu^{III}(OH_2)(OH_2)\right]^{6+} \longrightarrow \left[Ru^{IV}ORu^{IV}ORu^{IV}(OH)(OH)\right]^{6+} + 2e^- + 2H^+ \quad (12)$$

The change in slope to −90 mV/pH unit at 3.0 < pH <4.5 signals the first dissociation constant, pK_{a1}, for the oxidized trimer, and the net oxidation is

$$\left[Ru^{III}ORu^{IV}ORu^{III}(OH_2)(OH_2)\right]^{6+} \longrightarrow \left[Ru^{IV}ORu^{IV}ORu^{IV}(OH)(O)\right]^{5+} + 2e^- + 3H^+ \quad (13)$$

At 4.5 < pH < 7.0 $[(bpy)_2(OH)Ru^{III}ORu^{IV}(bpy)_2ORu^{III}(H_2O)(bpy)_2]^{5+}$ is the dominant form of the [III,IV,III] trimer, and the net oxidation is

$$\left[Ru^{III}ORu^{IV}ORu^{III}(OH)(OH_2)\right]^{5+} \longrightarrow \left[Ru^{IV}ORu^{IV}ORu^{IV}(OH)(O)\right]^{5+} + 2e^- + 2H^+ \quad (14)$$

At 7.0 < pH < 11.0, (slope −30 mV/pH unit), the net oxidation is

$$\left[Ru^{III}ORu^{IV}ORu^{III}(OH)(OH)\right]^{4+} \longrightarrow \left[Ru^{IV}ORu^{IV}ORu^{IV}(OH)(O)\right]^{5+} + 2e^- + H^+ \quad (15)$$

and in the most basic region, above pH 11.0, pK_{a2} for the [IV,IV,IV] trimer is reached (slope −60 mV/pH unit) and the oxidation becomes

$$\left[Ru^{III}ORu^{IV}ORu^{III}(OH)(OH)\right]^{4+} \longrightarrow \left[Ru^{IV}ORu^{IV}ORu^{IV}(O)(O)\right]^{4+} + 2e^- + 2H^+ \quad (16)$$

It is noteworthy that the oxidation of the [III,IV,III] state occurs by two electrons over the entire pH range, 0 < pH < 14. Thus, the one-electron intermediate redox state [III,V,III] or [III,IV,IV] is not thermodynamically stable at any accessible pH and is the only redox state of the trimer that is missing over the whole pH range.

The RDE data provide information on the electrode mechanism associated with the two-electron oxidation of the [III,IV,III] trimer. At pH 9.96, the oxidation displays a pronounced deviation from Levich behavior (Figure 4), but it displays only a slight deviation at pH 13. The appearance of pH-dependent rate behavior for these coupled proton and electron cases is quite common[7] but not well understood. An obvious possibility is the appearance of preceding, rate-limiting steps involving proton gain or loss from the complex.

4. Oxidation of the [IV,IV,IV] Trimer. There is a one-electron oxidation past the [IV,IV,IV] state to give [IV,V,IV]. As illustrated in Figure 6 the pH dependence observed for the redox potential of this additional couple can be understood on the basis of the formulation $[(bpy)_2(O)Ru^{IV}ORu^{V}(bpy)_2ORu^{IV}(O)(bpy)_2]^{5+}$ for the higher oxidation state and the pK_a values established for the [IV,IV,IV] oxidation state as described above.

Unfortunately, neither of the higher oxidation states is stable on the coulometric time scale. Although we have not yet documented the decomposition pathways involved, they appear to involve hydrolytic loss and/or oxidation of bpy ligands as for other

Table III. pK_a Values for the Ru–bpy Trimer,[a] Dimer, and Related Monomers in Different Oxidation States at μ = 0.1 M[b]

species	$pK_{a(hbl)}$[b]	$pK_{a(hb2)}$[b]	pK_{a1}	pK_{a2}	pK_{a3}	pK_{a4}
			Ru–bpy Trimer[c]			
[IV,V,IV]						<0
[IV,IV,IV]					3.0	11.5
[III,IV,III]			5.0[d]	6.8[d]		
[III,III,III]				<12		
[II,IV,II]		5.5 (?)	10.5			
[II,II,II]	10.5	11.5				
			Ru–bpy dimer[c,e]			
[V,V]						<0
[IV,V]						<2
[III,IV]			0.4	3.4	13.7[f]	
[III,III]	<0		5.9	8.3		
[II,II]	~9[g]					
			$[Ru(bpy)_2(py)(OH_2)]^{n+}$[h]			
[IV]				<0		
[III]			0.9	>13		
[II]			10.3			
			$[Ru(bpy)_2(OH_2)_2]^{n+}$[i]			
[VI]						<0
[V]						~6
[IV]					~5.5	>9
[III]			~2	~5.5	>9	
[II]			11.0[g]			

[a] pK_a values inferred from Figure 6 (see text). [b] hb1 and hb2 denote dissociation of first and second hydroxo-bridging protons. [c] Valence state designations of the Ru–bpy trimer and Ru–bpy dimer are described in text. [d] By glass-electrode titration. [e] Reference 3. [f] Reference 7a. [g] Reference 17. [h] Reference 18. [i] Reference 19.

polypyridyl Ru complexes.[15,16] The one-electron oxidation of [IV,IV,IV] shows a slight deviation from Levich behavior at pH 9.96 (Figure 4), perhaps because of an insufficient supply of [IV,IV,IV] produced in the chemically retarded two-electron oxidation of the [III,IV,III] state.

Summary of Redox and Acid–Base Properties. In addition to the Pourbaix diagram in Figure 6, the oxidation-state–proton-composition diagram in Figure 7 provides a useful summary of the redox and acid–base properties of the trimer. The proton compositions of the various couples are listed in increasing order on the vertical axis, and the various oxidation states are listed on the horizontal axis. The figure is essentially a two-dimensional Latimer diagram, with standard potentials for the proton-independent couples of the trimer listed horizontally, and acid dissociation constants listed vertically.

Some interesting features emerge from the array of data. One is how the coupled loss of electrons and protons tends to keep the total charge on the trimer relatively constant. The charge type varies between +2 and +6 for the entire range of pH and potentials despite a difference of seven electrons between the most reduced and most oxidized states. It is especially striking that at neutral pH, the charge on the complex rises only from +4 to +5 in the seven-electron oxidation of [II,II,II] to [IV,V,IV].

The change in proton content with electron content has as one of its origins electronic effects arising from the Ru–O interaction. Upon oxidation, the Ru sites become more electron deficient. Loss of protons from bound aqua or hydroxo ligands to give hydroxo or oxo groups, respectively, enhances both the σ- and π-donating ability of the bound O atom. The net effect is to stabilize the Ru sites by increased Ru–O mixing. Reduction to [II,II,II] leads to relatively electron-rich Ru sites and the electronic configuration $(d\pi)^6$. With the filling of the $d\pi$ levels there is no longer a basis for Ru–Ru interactions via $d\pi$(Ru)–p(O)–$d\pi$(Ru) mixing, and an orbital basis is created for protonation at the oxo bridges.

pK_a values for the Ru–bpy trimer in various redox states are summarized in Table III. Included for comparison are pK_a values for the Ru–bpy dimer, and the monomers $[(bpy)_2(py)Ru(OH_2)]^{n+}$ and $[(bpy)_2Ru(OH_2)_2]^{n+}$. A general trend of decreasing pK_a values with increasing oxidation state is visible in all four systems. This is an expected result since as their oxidation states increase, the metal centers draw negative charge from the ligands, making the groups bearing dissociable protons more acidic.

The values of pK_{a1} and pK_{a2} for the [III,IV,III] trimer and the [III,III] dimer are quite similar. This corroborates the formal assignment of oxidation states at the end ruthenium atoms in the trimer as Ru(III). It is interesting to compare pK_a values for related monomer, dimer, and trimer with regard to the "electron-withdrawing ability" of the "ligands" in the position cis to the bound H_2O group. If we represent the three species as $[(bpy)_2Ru^{III}(OH_2)OR]$, when R = H^+, pK_{a1} = 5.5; when R = $-Ru^{III}(bpy)_2(OH_2)$, pK_{a1} = 5.9; and when R = $-Ru^{IV}(bpy)_2ORu^{III}(bpy)_2(OH_2)$, pK_{a1} = 5.0. Thus the three groups have a similar electron-withdrawing ability.

Finally, pK_a values for the dissociation of hydroxo-bridge protons are similar for the [II,II,II] trimer and the [II,II] dimer. The values show that in the reduced forms of these complexes, hydroxo bridging is readily accessible although the hydroxo-bridged complexes do appear to hydrolyze readily in acidic solutions.

Spectral Properties. The main content of this paper was to document the extraordinarily rich redox chemistry of the trimer. Nonetheless, it is worthwhile to compare the UV–visible spectrum of the Ru–bpy trimer to that of the Ru–bpy dimer and also to the analogous tetradecaammine trimer (ruthenium red) and the decaammine dimer. Literature spectral data for the latter three complexes are summarized in Table II.

In comparing the diaqua Ru–bpy dimer to the diaqua Ru–bpy trimer, one sees that the energy of the prominent visible absorption band decreases from 15 700 to 15 310 cm^{-1}, and the extinction coefficient increases dramatically from 21 100 to 104 000 M^{-1} cm^{-1}. By comparison, upon going from the decaammine dimer to the tetradecaammine trimer, the band energy decreases from 19 800 to 18 000 cm^{-1}, and the extinction coefficient increases from 16 200 to 69 900 M^{-1} cm^{-1}. The transitions responsible for the bands in the bipyridyl and ammine complexes are undoubtedly closely related. The electronic structures of these and related cases are currently under investigation.

Reactivity. One of the reasons for our interest in the Ru–bpy trimer was the hope that its reactivity might shed light on the catalytic oxidations of water to O_2 and of chloride to Cl_2 by the Ru–bpy dimer. An electrochemical study of the dimer shows[3] that it has a complex but understandable oxidative chemistry based on a series of redox processes involving (1) a relatively low-potential, one-electron oxidation, [III,III] → [III,IV] + e^-, (2) above pH 2.2, a two-electron oxidation from [III,IV] to [IV,V]

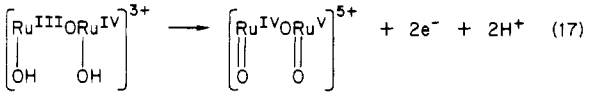

(17)

followed by a one-electron oxidation to [V,V]

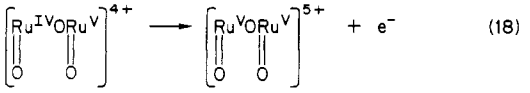

(18)

and, (3) below pH 2.2, direct three-electron oxidation of [III,IV] to [V,V].

In contrast to the dimer,[3] preliminary results show that when an excess of Ce(IV) is added to a solution (pH 1) containing the trimer, only small amounts of O_2 are produced and the trimer is decomposed. The trimer is not an oxidation catalyst even though [IV,V,IV] is thermodynamically a powerful oxidant. There are at least two possible reasons that may cause the difference in oxidative abilities of the dimer and trimer.

The first is that, in the dimer, intracoordination sphere coupling of the two terminal Ru-bound oxygen atoms might occur:

(16) Gosh, P. K.; Brunschwig, B. S.; Chou, M.; Creutz, C.; Sutin, N. *J. Am. Chem. Soc.* **1984**, *106*, 4772–4783.
(17) Geselowitz, D. A., unpublished results.
(18) Moyer, B. A.; Meyer, T. J. *Inorg. Chem.* **1981**, *20*, 436–444.
(19) Takeuchi, K., unpublished data.

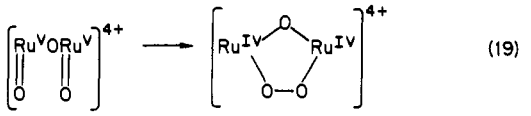

(19)

Such a pathway is not available to the trimer because of the $O-Ru^{IV}-O$ "spacer" between the $Ru-OH_2$ sites.

The second is that the [V,V] dimer is sufficiently strong as an oxidant that it can carry out the net four-electron oxidation of H_2O to O_2 by a single intramolecular step or by a series of sequential intramolecular steps as shown by the thermodynamics of water oxidation[3] by [V,V] at pH 1:

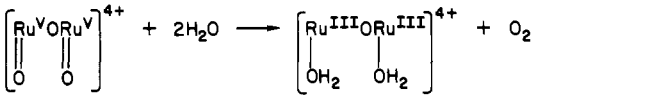

$E^{\circ\prime} = 0.25$ eV (20)

Even though the oxidized forms of the trimer have the thermodynamic ability to oxidize water to oxygen, for one molecule of the trimer to oxidize water in a four-electron step, the trimer must be reduced at least to the [II,III,II] state. For the Ru–bpy trimer at pH 1, calculated $E^{\circ\prime}$ values for the five-electron couple [IV,IV,IV]/[II,III,II] and the six-electron couple [IV,V,IV]/[II,III,II] are 0.7 and 0.8 V vs. SCE, respectively. Thermodynamically, neither couple is capable of oxidizing water for which $E^{\circ\prime} = 0.93$ V vs. SCE at pH 1.

Acknowledgment is made to X. B. Cox of this department for the measurement of XPS spectra. This research was supported by the National Institutes of Health under Grant No. 5-RO1-GM32296-02.

Registry No. $[Ru_3(bpy)_6O_2(OH_2)_2](ClO_4)_6$, 101954-90-9; $[Ru_3(bpy)_6O_2(OH_2)_2]^{9+}$, 101954-91-0; $[Ru_3(bpy)_6O_2(OH_2)_2]^{8+}$, 101954-92-1; $[Ru_3(bpy)_6O_2(OH_2)_2]^{5+}$, 101954-93-2; $[Ru_3(bpy)_6O_2(OH_2)_2]^{4+}$, 101695-59-4; $[Ru_3(bpy)_6O_2(OH_2)_2]^{3+}$, 101954-95-4; $[Ru_3(bpy)_6O_2(OH_2)_2]^{2+}$, 101954-94-3; $Ru(bpy)_2Cl_2$, 15746-57-3.

Contribution from the Department of Chemistry, The University of North Carolina, Chapel Hill, North Carolina 27514

Redox Properties of the Water Oxidation Catalyst $(bpy)_2(H_2O)RuORu(H_2O)(bpy)_2^{4+}$ in Thin Polymeric Films. Electrocatalytic Oxidation of Cl^- to Cl_2

William J. Vining and Thomas J. Meyer*

Received August 20, 1985

Chemically modified electrodes containing the ruthenium and osmium oxo-bridged dimers $[(bpy)_2(H_2O)M^{III}]_2O^{4+}$ (bpy = 2,2′-bipyridine) have been prepared by cation exchange into films of partially hydrolyzed *p*-chlorosulfonated polystyrene deposited onto glassy carbon electrodes. Both similarities and differences appear in comparing solution and film redox and acid–base properties: (1) As in solution the dimers undergo an initial one-electron oxidation, but the charge-transfer processes leading to higher oxidation states are inhibited in the polymeric film. (2) Reduction of the dimer leads to cleavage and formation of the monomers $(bpy)_2M(H_2O)_2^{2+}$ in the film. (3) In the film environment the dimers are less acidic than in solution. The catalytic oxidation of chloride ion by electrodes containing the Ru dimer has been studied in detail. Oxidation of a 1.0 M LiCl solution occurs with an initial current density of 100 mA/cm^2, and 26 000 turnovers/Ru site are obtained before deactivation of the catalyst occurs. Rotated-disk experiments show that the oxidation of Cl^- is independent of rotation rate but linearly dependent on $[Cl^-]$. Deactivation of catalyst appears to occur by oxidatively induced anation, possibly involving binding of sulfonate sites on the polymer to the dimer.

Introduction

Most of the work to date on the modification of electrode surfaces by the attachment of redox-active species either adsorbed or bound within an insoluble polymeric film has focused on simple electron-transfer processes.[1,2] A more demanding goal is the attachment of couples known to behave as redox catalysts in solution where, hopefully, some or all of the reactivity characteristics displayed in solution are retained in the environment of the polymeric film.

Redox reactions that occur by steps more complex than simple electron transfer are often beset with large overvoltages at electrode surfaces because of the inability of the electrode surface to meet the mechanistic demands of the reaction. Homogeneous redox catalysts have the advantage that they can be modified synthetically in a systematic fashion and detailed mechanistic studies can be carried out by using conventional techniques. If the reactivity characteristics of a solution catalyst can be maintained on an electrode surface or in a polymeric film, the possibility exists for developing electrode materials that operate with reactant specificity and decreased overvoltages. Some examples of redox catalysis based on surface-bound redox sites are known.[3-8]

Recently, it was shown that upon oxidation the μ-oxo-bridged Ru dimer $[Ru(bpy)_2(H_2O)]_2O^{4+}$ has the remarkable ability of catalyzing both the oxidation of water to dioxygen[9-11] and the oxidation of chloride to chlorine.[12] From the results of an electrochemical study it was concluded that oxidation of water may occur through a series of redox steps involving the loss of both protons and electrons with the final step being the loss of dioxygen and rebinding of two waters to the complex (eq 1, 2). Although the mechanistic details of the reaction are still under investigation, the key appears to be the final step where the highly oxidized Ru(V)–Ru(V) form of the dimer triggers the evolution of dioxygen. In addition, the Ru(V)–Ru(V) form of the dimer has been found to be a potent catalyst for the oxidation of Cl^- to Cl_2.

We report here on the redox and catalytic properties of the Ru dimer ion exchanged into the cation-exchange materials polystyrenesulfonate and Nafion. Our interest in the system was in comparing its reactivity properties in the polymeric film envi-

(1) Murray, R. W. *Acc. Chem. Res.* **1980**, *13*, 135.
(2) Murray, R. W. *Electroanal. Chem.* **1984**, *13*, 190.
(3) Calvert, J. M.; Meyer, T. J. *Inorg. Chem.* **1982**, *21*, 3978.
(4) Kutner, W.; Meyer, T. J.; Murray, R. W. *J. Electroanal. Chem. Interfacial Electrochem.* **1985**, *195*, 375.
(5) McHatton, R. C.; Anson, F. C. *Inorg. Chem.* **1984**, *23*, 3935.
(6) Buttry, D. A.; Anson, F. C. *J. Am. Chem. Soc.* **1984**, *106*, 59.
(7) Collman, J. P.; Marrocco, M.; Denisevich, P.; Koval, C.; Anson, F. C. *J. Electroanal. Chem. Interfacial Electrochem.* **1979**, *101*, 117.
(8) Samuels, G. J.; Meyer, T. J. *J. Am. Chem. Soc.* **1981**, *103*, 307.
(9) Gersten, S. W.; Samuels, G. J.; Meyer, T. J. *J. Am. Chem. Soc.* **1982**, *104*, 4029.
(10) Honda, K.; Frank, A. J. *J. Chem. Soc., Chem. Commun.* **1984**, 1635.
(11) Gilbert, J. A.; Eggleston, D. S.; Murphy, W. R.; Geselowitz, D. A.; Gersten, S. W.; Hodgson, D. J.; Meyer, T. J. *J. Am. Chem. Soc.* **1985**, *107*, 3855.
(12) (a) Ellis, C. D.; Gilbert, J. A.; Murphy, W. R.; Meyer, T. J. *J. Am. Chem. Soc.* **1983**, *105*, 4842. (b) Vining, W. J.; Meyer, T. J. *J. Electroanal. Chem. Interfacial Electrochem.* **1985**, *195*, 183–187.

0020-1669/86/1325-2023$01.50/0